Experimental and Theoretical Studies of the Reactions Y (a^2D) + H_2CO and Y (a^2D) + CH_3CHO

Jonathan J. Schroden,[†] H. Floyd Davis,*[,†] and Craig A. Bayse*[,‡]

Department of Chemistry and Chemical Biology, Cornell University, Ithaca, New York 14853, and Department of Chemistry and Biochemistry, Old Dominion University, Hampton Blvd., Norfolk, Virginia 23529

Received: June 29, 2007; In Final Form: August 14, 2007

The reactions of ground state Y (a^2D) with H_2CO and CH_3CHO were studied at a range of collision energies in crossed molecular beams. For reaction with H_2CO, three product channels were observed: formation of YH_2 + CO, YCO + H_2, and YHCO + H. Reaction with CH_3CHO led to three analogous product channels involving formation of $HYCH_3$ + CO, YCH_2CO + H_2, and YCH_3CO + H. The calculated CCSD(T) energetics and DFT geometries for key intermediates in both reactions, together with RRKM theory, are used to calculate *a priori* the branching ratios between various product channels. These calculated values are compared to those obtained experimentally.

I. Introduction

The large number of experimental and theoretical studies of reactions of neutral, gas-phase transition metal atoms with hydrocarbon molecules has led to a better understanding of fundamental aspects of elementary transition metal reactions initiated by C−H bond insertion.[1−5] The combination[1,2] of *ab initio* calculations at the PCI-80 level with kinetics measurements and Rice−Ramsperger−Kassel−Marcus theory (RRKM) for the reactions M + CH_4, C_2H_6, c-C_3H_6, and C_2H_4 (where M is each of the second-row transition metal atoms) provided insight into the trends in the heights of potential energy barriers for C−H and C−C bond insertion, as well as for subsequent steps leading to elimination of molecular products. The agreement between the *ab initio* calculations and the kinetics data suggested that the calculated energetics were accurate to within 2−3 kcal/mol.[1] Subsequent experimental studies in our laboratory on the Y + C_2H_2,[6] Y + C_2H_6,[7] and Zr + C_2H_4[8] reactions have shown that following C−H insertion, several competing reaction pathways may occur. In cases where C−C insertion is competitive, such as in the M + cyclopropane reaction (where M = Y, Zr, Nb, Mo), the measured branching ratios between MCH_2 + C_2H_4 and MC_3H_4 + H_2 products were found to correlate with the relative C−C and C−H insertion barrier heights predicted theoretically.[9]

Weisshaar and co-workers have combined kinetics studies with density functional theory (DFT) to examine the Y[5] and Zr[3,4] + C_2H_4 reactions in detail. In the Zr calculations, the role of the singlet excited state surface was considered explicitly,[4] and a number of different reaction mechanisms for elimination of H_2 were explored. Several functionals were compared, with the conclusion that the popular functional B3LYP consistently overestimated the energies of key transition states by 6−9 kcal/mol, whereas the mPW1PW91 functional gave results in closer agreement with experimental results.[4,5]

We have investigated reactions of ground state yttrium atoms with carbonyl-containing molecules, most notably formaldehyde,[10−12] acetaldehyde,[12] acetone,[12] and ketene.[13] The calculated energetics of the Y + H_2CO reaction, as determined by Bayse using single-reference and multireference techniques, are shown in Figure 1.[11] The calculations predicted that CO elimination should be the most exoergic channel, with H_2 elimination products lying slightly higher in energy. A third product channel, involving H atom elimination, was calculated to be 15.7 kcal/mol endoergic.[11] Experimentally, all three reaction channels were observed.[10,12] A large fraction of the available energy was found to be deposited into product translational energy for H_2 and CO elimination.[10,12] In the case of H_2 elimination, this was consistent with the prediction of a barrier in the exit channel.[10] It was found experimentally that the dominant channel was CO elimination,[10,12] consistent with this channel being thermodynamically favored.[11]

Although results for Y + H_2CO and Y + H_2CCO have been discussed in some detail,[10−14] a previous study of Y + CH_3CHO focused only on the CO elimination channel.[12] The purpose of the present paper is to present new DFT and *ab initio* calculations focusing on the detailed mechanisms for the competing reaction pathways, as well as a more complete account of the Y + CH_3CHO experimental study. The CCSD(T) energetics and DFT geometries for both the Y + H_2CO and Y + CH_3CHO reactions are employed in RRKM calculations of the branching ratios between various product channels from these reactions. The calculated values are compared to those obtained experimentally, allowing us to test the ability of theory to accurately predict the energies of important stationary points for these model neutral transition metal atom reactions.

II. Experimental Section

The experiments were carried out using a rotatable source crossed molecular beams apparatus.[15] The atomic metal beam was prepared by focusing the 532 nm output (15 mJ/pulse, 1 mm diameter) from a Nd:YAG laser (Continuum Surelite) onto a 0.25 in. diameter yttrium rod (Alfa Aesar, 99.9%). The ablated metal atoms were entrained in a pulse of inert carrier gas[16] delivered by a piezoelectric pulsed valve.[17] The resulting metal beam was collimated via a skimmer, defining aperture, and chopper wheel before being crossed at a fixed right-angle

* To whom correspondence should be addressed. E-mail: H.F.D., hfd1@cornell.edu; C.A.B., cbayse@odu.edu.
† Cornell University.
‡ Old Dominion University.

10.1021/jp075090+ CCC: $37.00 © 2007 American Chemical Society
Published on Web 10/17/2007

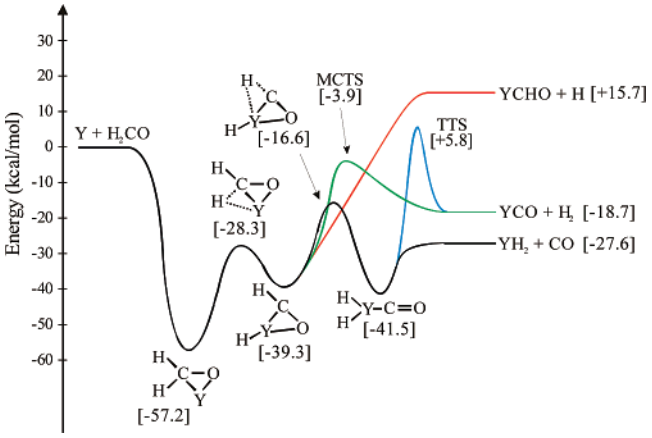

Figure 1. Energetics for the Y (a^2D) + H_2CO reaction as calculated using single-reference and multireference techniques. Adapted from ref 11.

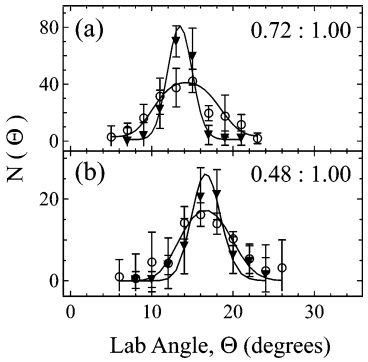

Figure 2. Lab angular distributions for YCHO (solid triangles) and YCO (open circles) products from the Y + H_2CO reaction at (a) E_{coll} = 30.3 kcal/mol and (b) E_{coll} = 27.0 kcal/mol. Distributions have been scaled to the same number of scans. Product branching ratio, ϕ_{YCHO}: ϕ_{YCO}, included in upper right corners.

geometry by a molecular beam. This beam was generated by passing 5 psig of an inert carrier gas through a bubbler containing the molecular reactant, either solid paraformaldehyde (Aldrich, 95%) or liquid acetaldehyde (Aldrich, 99%). The bubbler containing the molecular reactant was held at a fixed temperature using either a silicon oil or methanol bath. The velocity distributions of both beams were measured by modulating the beams using a slotted chopper wheel and monitoring their time-of-flight (TOF) to the detector using electron impact ionization.[15] Relevant beam parameters can be found in Table 1. The yttrium beam has been characterized previously, and consisted only of ground state Y ($a^2D_{1/2}$ and $a^2D_{3/2}$) atoms.[6]

The intersection of the two beams at right angles under high-vacuum conditions ($<1 \times 10^{-6}$ Torr) resulted in single, bimolecular collisions between the metal atoms and the molecular reactant. These collisions either led to reaction or to nonreactive scattering. In either case, the products of the collisions drifted 24.1 cm to the triply differentially pumped detector, where they were ionized with the 157 nm output from a pulsed F_2 excimer laser.[15] Product TOF spectra were obtained by scanning the delay time of the excimer laser pulse with respect to a time zero, defined by the chopper wheel. Rotation of the beams with respect to the fixed detector allowed product TOF spectra to be taken at different laboratory angles. Integration of these spectra led to a laboratory angular distribution, $N(\Theta)$. The TOF spectra and lab angular distribution were simulated using a forward-convolution method,[18] which required the input of two center-of-mass (CM) distributions, the translational energy release distribution, $P(E)$, and the CM angular distribution, $T(\theta)$. These two input functions were iteratively adjusted until optimal agreement was reached between the simulated and experimental data.

III. Computational Details

a. Electronic Structure Calculations. Theoretical calculations were performed in two basis sets using the Gaussian 03 software package.[19] Multicenter transition states (MCTS) were found using the partitioned rational function optimization procedure in GAMESS-UK.[20] Basis set I (BSI) uses the Dunning cc-pVDZ basis sets[21] on carbon, hydrogen, and oxygen and the relativistic ECP basis[22] of Lajohn et al. (EC-RECP) on yttrium (5s5p4d)/[3s3p3d]. The metal basis set includes Couty and Hall's improved $(n+1)$p coefficients.[23] BSII uses the Dunning cc-pVTZ basis[24] on carbon, hydrogen, and oxygen minus the f polarization functions on the heavy atoms and the d polarization functions on hydrogen. The metal is represented in BSII by the EC-RECP basis set uncontracted slightly for additional flexibility. Even-tempered diffuse s, p, and d functions and a set of STO-3G f-type polarization functions[25] contracted 21 are also added to the metal for a final representation of (6s6p5d3f)/[5s5p5d2f]. Geometries were optimized using unrestricted B3LYP[26] Kohn−Sham orbitals.[27] Vibrational frequencies and zero point energy (ZPE) corrections were calculated in BSI and BSII. Energies were recalculated at the coupled cluster level (CCSD(T))[28] from the B3LYP/BSII geometries.

b. RRKM Calculations. Rice−Ramsperger−Kassel−Marcus (RRKM) theory defines the microcanonical unimolecular rate constant as

$$k_{uni}(E,J) = \frac{W^{\dagger}(E,J)}{h\rho(E,J)} \qquad (9)$$

where $W^{\dagger}$ is number of open rovibrational states at the transition state, ρ is the density of rovibrational states of the bound complex, and h is Planck's constant.[29] The energy, E, is equal to the total amount of energy available to the complex, which is taken to be the sum of the collision energy and the dissociation energy of the complex relative to ground state reactants (i.e., $E = E_{coll} + D_0$). Although there is some vibrational energy in the formaldehyde and acetaldehyde reactants[30] (most notably for acetaldehyde, with its low-frequency torsional mode,[31] $\nu = 50$ cm^{-1}), this is not expected to contribute more than 1−2 kcal/mol of energy for reaction and was neglected. The total angular momentum of the collision, J, is assumed to be conserved throughout the reaction and results exclusively from the orbital angular momentum of the collision because the rotational energies of the molecular reactants are negligible for jet-cooled reactants. Reaction rate constants are calculated using a standard program.[32] The inputs for RRKM calculations include the CCSD(T) energies, and DFT/BSII vibrational frequencies and moments of inertia of both the intermediates and transition states.[11,33] Dissociation to YRCO + H was modeled as a loose transition state; all other barriers were modeled as tight. The potential for H loss was approximated using a Morse potential including a repulsive centrifugal term, $h^2J(J+1)/8\pi^2\mu R^2$. A distribution of angular momenta, $P(J) = 2J/J_{max}^2$, was assumed to model the crossed molecular beams experiment.

IV. Experimental Results

a. Y(a^2D) + H_2CO. Results of the Y + H_2CO reaction have already been published.[10,12] New data were taken at E_{coll} = 27.0 and 30.3 kcal/mol with the focus of the present study being the

TABLE 1: Experimental Conditions for Y + H_2CO, CH_3CHO Reactions

Y + H_2CO

E_{coll}[a]	Y carrier gas	Y beam velocity[b]	Y beam fwhm[b]	H_2CO carrier gas	H_2CO temp[c]	H_2CO beam velocity[b]	H_2CO beam fwhm[b]
27.0	He	2350	305	H_2	98	2000	203
30.3	50% He/50% H_2	2700	346	H_2	98	2000	203

Y + CH_3CHO

E_{coll}[a]	Y carrier gas	Y beam velocity[b]	Y beam fwhm[b]	CH_3CHO carrier gas	CH_3CHO temp[c]	CH_3CHO beam velocity[b]	CH_3CHO beam fwhm[b]
7.1	Ar	1000	103	50% He/50% Ne	0	990	166
9.3	Ne	1250	132	50% He/50% Ne	0	990	166
11.0	Ne	1250	132	He	−10	1200	196
13.1	50% He/50% Ne	1515	159	He	−10	1200	196
15.9	50% He/50% Ne	1515	159	He	−28	1470	162
26.8	He	2290	316	He	−28	1470	162
27.7	He	2290	316	50% He/50% H_2	−28	1600	184

[a] In kcal/mol. [b] In m/s. [c] In °C.

TABLE 2: Energies of B through T Relative to the Reactant Asymptote for Y + Acetaldehyde

		B3LYP/BSI	B3LYP/BSII	CCSD(T)/BSII
B	Y(MeHCO)	−49.17	−50.55	−51.95
C	TS_{CC}	−18.84	−20.76	−22.42
D	$TS_{\alpha CH}$	−29.55	−28.78	−28.77
E	MeYHCO	−39.90	−40.87	−42.32
F	HYMeCO	−42.16	−40.57	−42.02
G	$TS_{CC'}$	−14.52	−14.96	−15.65
H	TS_{CH}	−21.66	−23.52	−24.43
I	$TS_{CH''}$	−5.55	−6.06	−6.15
J	MCTS-I	7.86	7.17	6.61
K	MeHYCO	−41.15	−42.41	−42.41
L	$H_2Y(OCCH_2)$	−36.70	−36.39	−37.38
M	H_2 + $Y(OCCH_2)$	−26.03	−29.25	−28.90
N	$HYCH_3$ + CO	−23.26	−24.41	−30.01
O	H + YMeCO	18.67	21.18	13.13
P	$TS_{\beta CH}$	−33.77	−35.10	−35.32
Q	$HY(OCHCH_2)$	−57.13	−57.77	−58.24
R	$TS_{CH'''}$	−19.06	−19.64	−15.76
S	MCTS-II	−22.86	−24.87	−23.90
T	H + $Y(OCHCH_2)$	−4.62	−3.15	−8.97

TABLE 3: Experimental and Simulated Branching Ratios between CO, H and H_2 Elimination for Y + H_2CO, CH_3CHO Reactions

E_{coll}[a]	k_{CO} (10^{13} s^{-1})	k_H (10^9 s^{-1})	k_{H_2} (10^9 s^{-1})	RRKM ϕ_{YCHO}:ϕ_{YCO}[b]	experimental ϕ_{YCHO}:ϕ_{YCO}
27.0	1.70	1.71	3.60	0.48:1.00	0.48:1.00
30.3	6.18	2.86	4.82	0.59:1.00	0.72:1.00

[a] In kcal/mol.; [b] Calculated as k_H:k_{H_2}.

determination of the product branching ratios for the competing channels (Tables 1 and 3−5). Four processes were observed:

$$Y + H_2CO \rightarrow YCHO\ (m/e\ 118) + H \quad (1)$$

$$\rightarrow YCO\ (m/e\ 117) + H_2 \quad (2)$$

$$\rightarrow YH_2\ (m/e\ 91) + CO \quad (3)$$

$$\rightarrow Y\ (m/e\ 89) + H_2CO \quad (4)$$

The TOF spectra for all four processes at E_{coll} = 27.0 and 30.3 were qualitatively similar to those shown previously.[10,12] The H:H_2 elimination product branching ratio, ϕ_{YCHO}:ϕ_{YCO}, was measured at each collision energy and is given in Table 3. Product fragmentation patterns and factors related to the transformation of data from the lab frame to the CM frame were explicitly taken into consideration when determining the product branching ratios. The observed signal levels for the YH_2 + CO channel were approximately 50 times greater than for the YCO + H_2 channel. However, due to the small mass of H_2, the YCO products are constrained to appear over a narrow angular range, enhancing our ability to observe this channel at laboratory angles near the CM angle. Assuming that the 157 nm photoionization cross-sections for each product were equal, our analysis indicates that the YH_2 + CO yield is 1000−2000 times greater than for YCO + H_2, *i.e.*, that the YCO + H_2 and YHCO + H channels each account for ≤0.05% of the products.

b. Y(a^2D) + CH_3CHO. The reaction of Y with acetaldehyde was studied at seven collision energies (Table 1); the following four processes were observed:

$$Y + CH_3CHO \rightarrow YCH_3CO\ (m/e\ 132) + H \quad (5)$$

$$\rightarrow YCH_2CO\ (m/e\ 131) + H_2 \quad (6)$$

$$\rightarrow HYCH_3\ (m/e\ 105) + CO \quad (7)$$

$$\rightarrow Y\ (m/e\ 89) + CH_3CHO \quad (8)$$

The CO elimination channel, which is again the dominant reaction at all collision energies, has been discussed in detail previously.[12] The TOF spectra for each process looked qualitatively similar at each collision energy, so representative data are shown only for E_{coll} = 11.0 kcal/mol. The TOF spectra for YCH_3CO and YCH_2CO products at this collision energy are shown in Figure 3. The spectra corresponding to H elimination are much narrower than those for H_2 elimination, largely because H_2 elimination is exothermic and H elimination is endothermic. The factor of 2 increase in the mass of the recoiling counter-fragment also contributed to the larger scattering sphere for YCH_2CO. Some fragmentation (23.5%) of the YCH_3CO product (*m*/*e* 132) to the mass of the YCH_2CO product (*m*/*e* 131) was observed. The degree of fragmentation was determined at the highest collision energy studied, E_{coll} = 27.7 kcal/mol, at which the data taken at *m*/*e* 131 were observed to be identical in shape to the data taken at *m*/*e* 132, but at 23.5% of the signal intensity. This indicated that the signal at *m*/*e* 131 was a result of fragmentation of YCH_3CO products and overflow of signal from *m*/*e* 132 to *m*/*e* 131 due to imperfect mass resolution of the detector. To correct for this, 23.5% of the YCH_3CO product signal has been subtracted from the corresponding YCH_2CO data at all collision energies. The laboratory angular distributions for YCH_3CO and YCH_2CO products are shown in Figure 4,

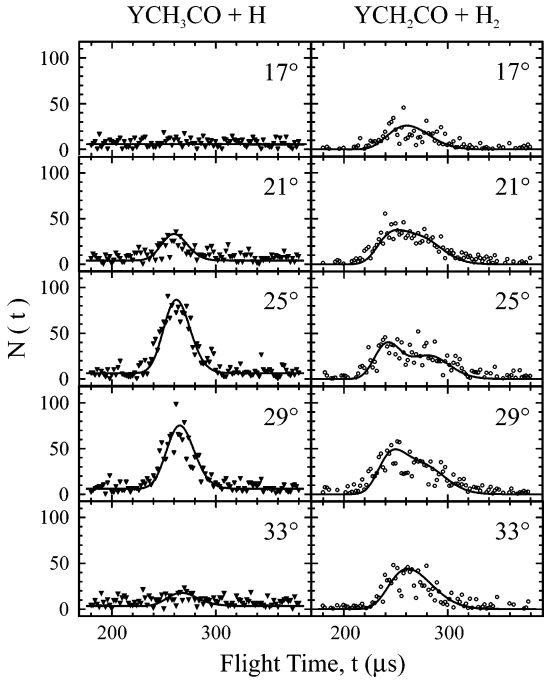

Figure 3. Time-of-flight spectra for YCH_3CO (solid triangles) and YCH_2CO (open circles) products from the Y + CH_3CHO reaction at indicated lab angles for E_{coll} = 11.0 kcal/mol. Spectra have been scaled to the same number of scans. Solid-line fits generated using the CM distributions shown in Figure 5.

along with the lab angular distributions for the same products at several other collision energies. At each collision energy, YCH_2CO products were spread over a wider range of laboratory angles than YCH_3CO products, for the same reasons as discussed above for the TOF spectra. The experimentally determined branching ratios, ϕ_{YCH_3CO}:ϕ_{YCH_2CO}, are given in Figure 4 for each collision energy.

The solid-line fits to the data in Figure 3 and Figure 4d were generated using the CM distributions shown in Figure 5. The CM angular distributions were symmetric about θ = 90°, suggesting that both the H and H_2 elimination reactions proceed via long-lived complexes, i.e., complexes that survived for several rotational periods. The CM angular distributions are isotropic, as expected from angular momentum considerations.[34] Also shown in Figure 5 are the translational energy release distributions. The $P(E)$ for H_2 elimination peaks further away from the zero of kinetic energy than that for H elimination, indicating that a greater amount of the available energy is deposited into kinetic energy of the YCH_2CO products than for YCH_3CO.

The TOF spectra for nonreactively scattered yttrium atoms from the Y + CH_3CHO reaction at E_{coll} = 26.8 kcal/mol are shown in Figure 6. At small lab angles, there is only one peak in the spectra, but at larger angles a second, slower peak appears. The corresponding lab angular distribution is shown in Figure 7. To fit these data, it was necessary to use a combination of two sets of CM distributions, which are shown in Figure 8. One set of CM distributions (Figure 8, left panels) contained a sharply forward-peaked $T(\theta)$, which is indicative of glancing (or large impact parameter) collisions. The other set (Figure 8, right panels) contained a forward−backward symmetric $T(\theta)$, which is indicative of formation of a long-lived complex. The $P(E)$'s for each set were similar in shape, with $\langle P(E)\rangle$ = 14.0 kcal/mol for the $P(E)$ corresponding to the forward-scattered $T(\theta)$ and $\langle P(E)\rangle$ = 13.1 kcal/mol for that corresponding to the forward−backward symmetric $T(\theta)$. These values indicate that both

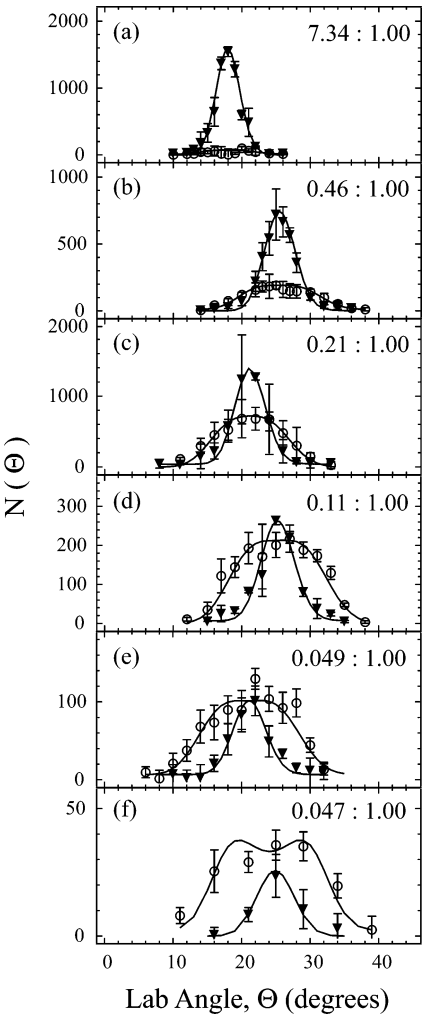

Figure 4. Lab angular distributions for YCH_3CO (solid triangles) and YCH_2CO (open circles) products from the Y + CH_3CHO reaction at (a) E_{coll} = 26.8 kcal/mol, (b) E_{coll} = 15.9 kcal/mol, (c) E_{coll} = 13.1 kcal/mol, (d) E_{coll} = 11.0 kcal/mol, (e) E_{coll} = 9.3 kcal/mol, and (f) E_{coll} = 7.1 kcal/mol. Distributions have been scaled to the same number of scans. Product branching ratio, ϕ_{YCH_3CO}:ϕ_{YCH_2CO}, included in upper right corners.

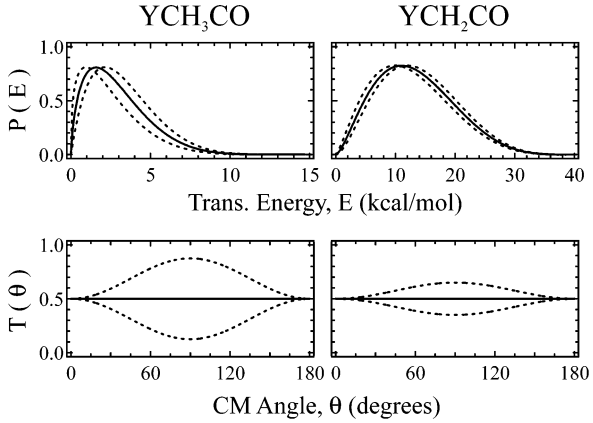

Figure 5. Center-of-mass distributions used to fit the YCH_3CO and YCH_2CO data from the Y + CH_3CHO reaction shown in Figures 3 and 4d for E_{coll} = 11.0 kcal/mol. Dashed lines indicate the range of distributions that give acceptable fits to the data (analogous to error bars).

nonreactive processes transfer approximately 50% of the initial reactant energy into acetaldehyde rotational and vibrational degrees of freedom.

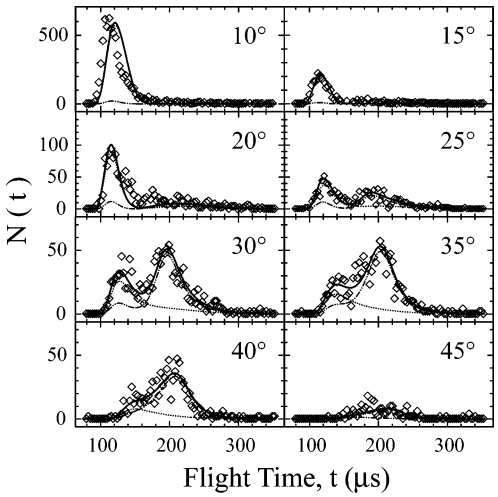

Figure 6. Time-of-flight spectra for nonreactively scattered Y atoms from the Y + CH_3CHO reaction at indicated lab angles for E_{coll} = 26.8 kcal/mol (open diamonds). Solid-line fits generated by summing the dotted line and dash-dot line contributions. Dotted lines generated using the CM distributions shown in Figure 8, left panels. Dash-dot lines generated using the CM distributions shown in Figure 8, right panels.

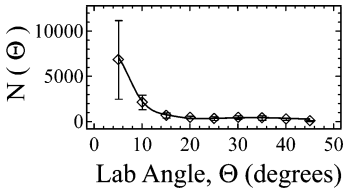

Figure 7. Lab angular distribution for nonreactively scattered Y atoms from the Y + CH_3CHO reaction at E_{coll} = 26.8 kcal/mol (open diamonds). Solid-line fit generated using the CM distributions shown in Figure 8.

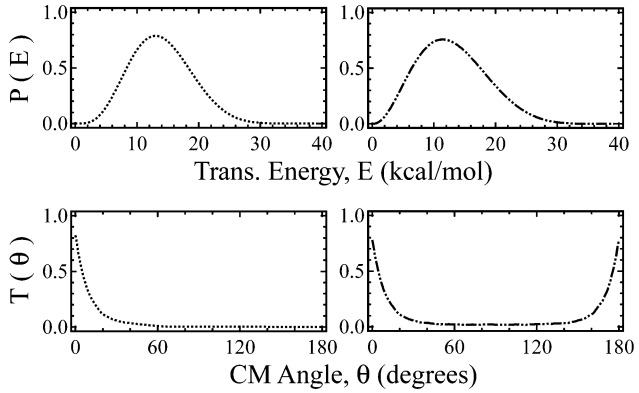

Figure 8. Center-of-mass distributions used to generate the fits to the nonreactive scattering data shown in Figures 6 and 7. Dashed line and dash-dot line distributions correspond to dashed line and dash-dot line fits in Figure 6, respectively.

The competition between elimination of H and H_2 was monitored as a function of collision energy for both the Y + H_2CO and Y + CH_3CHO reactions. The branching ratios between these product channels for each collision energy are shown in Figure 2 for Y + H_2CO and in Figure 4 for Y + CH_3CHO and listed in Tables 3−5. It would have been desirable to measure the $HYCH_3$ + CO yield as a function of collision energy. Unfortunately, YO impurity in the beam, which appears at the same *m*/*e* ratio as $HYCH_3$, made this impossible. Therefore, experiments were carried out using deuterated acetaldehyde, CD_3CDO, at a collision energy of 24.6 kcal/mol, leading to production of $DYCD_3$ + CO with a measured yield of ≈50%.

V. Comparison with Theoretical Results

a. Y(a^2D) + H_2CO. A theoretical study of the Y(a^2D) + H_2CO reaction has been published previously[11] (Figure 1). The reaction was assumed to proceed via initial formation of a π-complex followed by C−H insertion to HYHCO. Branching to the three products (CO loss, H_2 loss, and H loss) occurs from this intermediate. Over the course of the present study, a new transition state for the second hydride shift leading to CO loss was found. The activation energy for this species is −16.6 kcal/mol below the reactant asymptote, ∼10 kcal/mol below the TS reported in ref 11. This new TS, shown as **Z** in Figure 9, is also significantly lower than those for the H and H_2 loss pathways.

The RRKM rates for formation of the Y + H_2CO products were calculated on the basis of the TS for the three steps, starting from the intermediate HYHCO using theoretical data from ref 11. The hydride shift TS (−16.6 kcal/mol in Figure 1) was used to determine the RRKM rate constant for CO loss because the product, H_2YCO, decomposes to YH_2 + CO in a barrierless process. A loose transition state was assumed for H atom dissociation. The RRKM rate constants and branching ratios are listed in Table 3. The low barrier for the hydride shift gives a rate constant $k_{\beta H}$ 4 orders of magnitude greater than those for H_2 and H loss. This very large predicted preference for CO loss is in excellent agreement with the experimental measurements, which predicted that the YH_2:YCO branching ratio was 1000−2000:1 Because the signal levels from these two channels differ greatly, it is difficult to ensure that our detection sensitivity is linear over many orders of magnitude. Also, the ratio of the absolute ionization cross sections for the two channels are not accurately known and were assumed to be unity. In light of these uncertainties, we believe that the calculated YH_2:YCO branching ratio of 10^4 is in reasonable agreement with the measured value of $(1-2) \times 10^3$. The RRKM rates and branching ratios for H to H_2 loss are shown in Table 3. These values, 0.48:1 and 0.59:1 at E_{coll} = 27.0 and 30.3 kcal/mol are also in reasonable agreement with experiment, with the H loss channel increasing at higher collision energies.

b. Y(a^2D) + CH_3CHO. The proposed mechanism for the reaction of Y + acetaldehyde (Figure 10) involves three reactive pathways originating from the π-complex **B**: initial C−C insertion (path I), initial α-C−H insertion (path II), and β-C−H insertion (path III). The energies of the intermediates and transition states of these three pathways relative to the reactant asymptote are listed in Table 2. The energies stated within the text are at the CCSD(T)/BSII//B3LYP/BSII level corrected for zero point energy. The potential energy curves for the three pathways are shown in Figures 11−13. Selected geometric data (B3LYP/BSII) are shown in Figure 9.

Initial C−C insertion (Figure 10 (path I), Figure 11) leads to the major product $HYCH_3$ + CO in a series of steps analogous to CO loss in Y + H_2CO. A β-hydride shift from the formyl group of the CC insertion product **E** gives the methyl hydride **K**, which decomposes in a barrierless process to $HYCH_3$ + CO. The CC insertion transition state **C** is the largest barrier encountered along this reaction pathway and is the highest barrier found at the entrance of any of the three paths I−III.

The initial α-C−H insertion, Figure 10 (path II) and Figure 12, forms acetyl hydride **F**, from which a subsequent methyl shift gives **K** to form the CO elimination products, thus partially

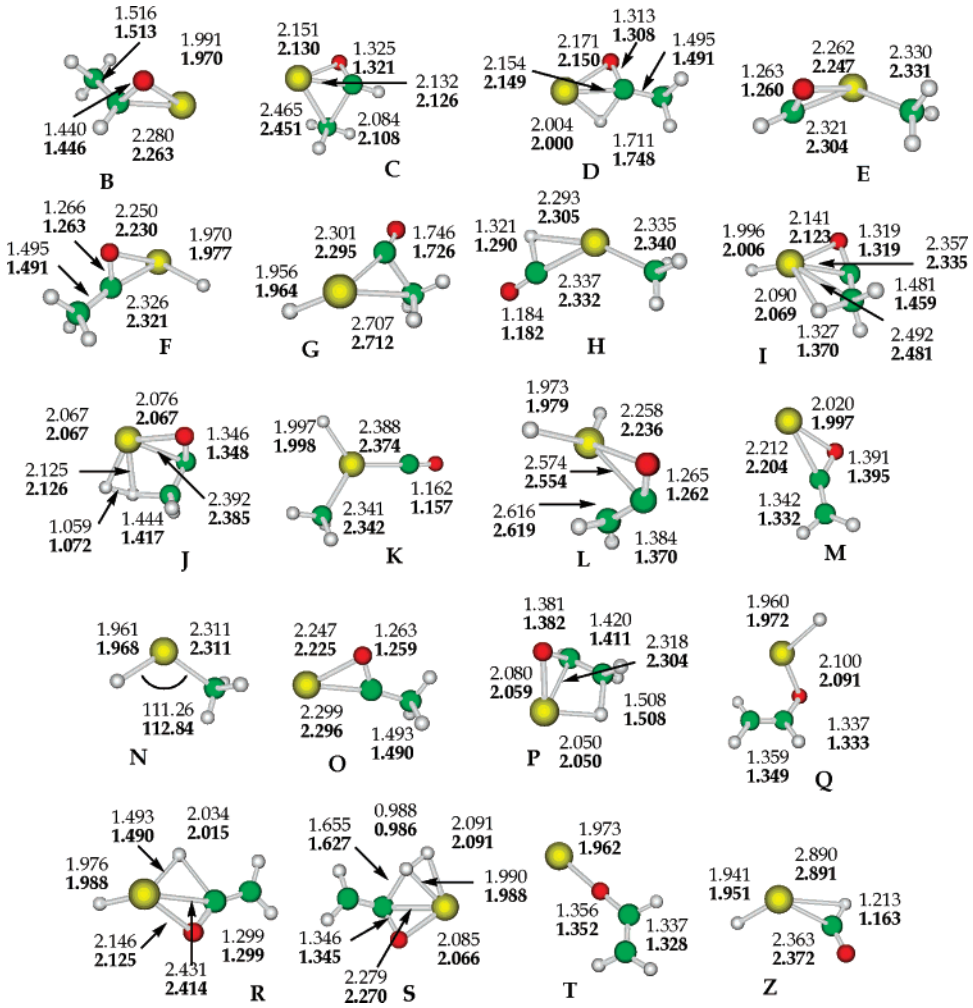

Figure 9. Selected geometric parameters for stationary points and transition states for the reaction of yttrium and acetaldehyde. Bond lengths are given in Ångstroms.

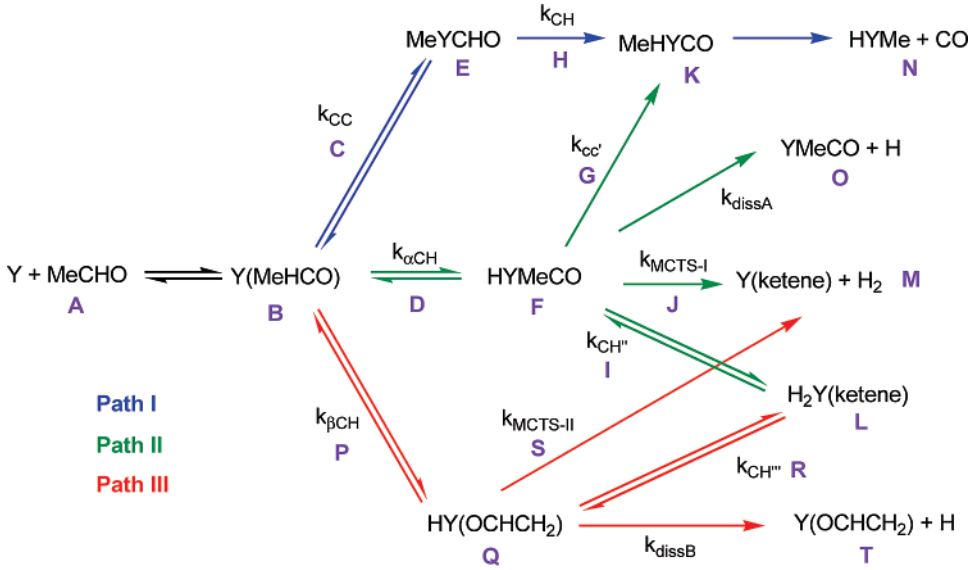

Figure 10. Competing pathways following formation of π-complex (B).

paralleling path I. The transition state for initial α-CH insertion **D** is lower than that of C−C insertion, but the products of each are similar energetically and slightly more stable than HYCHO (−39.29 kcal/mol). $TS_{\alpha CH}$ **D** is similar structurally to its counterpart in the Y + H_2CO mechanism although its barrier is ∼9 kcal/mol lower and the C−H bond being cleaved is shorter (1.748 Å vs 1.841 Å). Whereas the CH bond dissociation energies are similar for H_2CO and MeHCO, the activation barriers for α-C−H insertion by Y are lower for MeHCO due to the donation of electron density from the methyl group to the carbonyl carbon. The α-C−H insertion product **F** in path II can undergo several processes other than the reaction to form

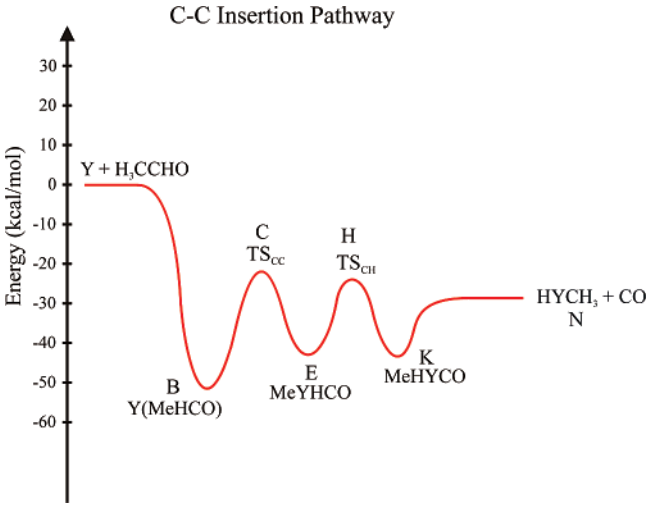

Figure 11. Energetics of path I, C− C insertion.

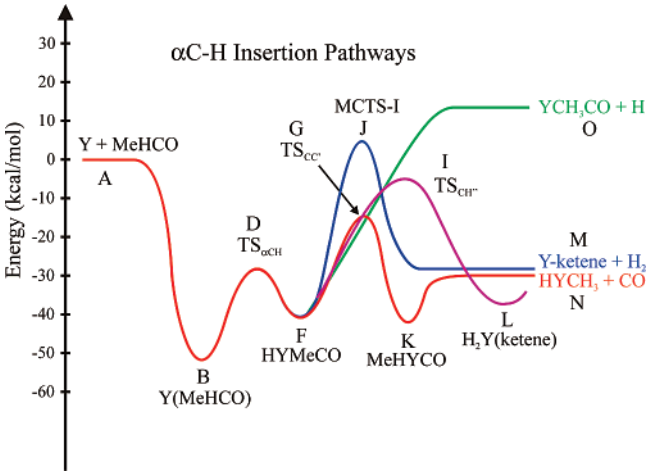

Figure 12. Energetics of path II, α-C−H insertion.

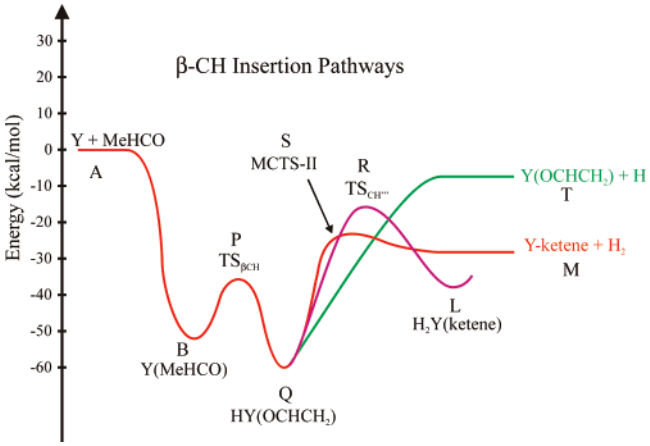

Figure 13. Energetics of path III, β-C−H insertion.

K. The simplest of these is the cleavage of the Y−H bond of **F** forming YMeCO + H **(O)**, a highly endothermic process requiring 13.13 kcal/mol above the reactant asymptote. Shift of a hydrogen atom from the acetyl ligand to the metal can occur through β-hydride transfer **I** to Y(H)$_2$(ketene) **L.** Alternatively, a multicentered TS (MCTS) **J** yields the products Y(ketene) + H_2. Attempts to model the Y(H_2)(ketene) product expected from the MCTS were unsuccessful and resulted in dissociation to **M**. The TS for β-hydride transfer $TS_{CH''}$ **I** is lower than $MCTS_I$ **J**, but both of these are high ($MCTS_I$ lies 6.61 kcal/mol above the reactant asymptote) because the ketene ligand is being formed in a high energy state as its CH_2 is twisted by ∼90° relative to the product conformation. Formation of **L** has been modeled as an equilibrium process, because the barrier to direct reductive elimination of H_2 from **L** is likely to involve a rather high barrier, as in the case of H_2 elimination from H_2-YCO in the formaldehyde reaction.[11]

TABLE 4: RRKM Rate Constants Calculated from the CCSD(T)/BSII Energies and B3LYP/BSII Frequencies

E_{coll}	k_{CC} (10^8 s^{-1})	$k_{\alpha CH}$ (10^9 s^{-1})	$k_{\beta CH}$ (10^{10} s^{-1})	$k_{CH'''}$ (10^6 s^{-1})	$k_{MCTS-II}$ (10^6 s^{-1})	k_{dissB} (10^6 s^{-1})
7.1	8.28	3.56	1.15	4.47	7.95	1.93
9.3	10.81	4.43	1.30	7.18	10.4	3.48
11.0	12.89	5.13	1.40	10.4	12.9	5.64
13.1	16.04	6.16	1.54	15.2	16.8	9.42
15.9	21.38	7.50	1.77	26.4	23.6	17.31
26.8	52.63	17.10	2.74	12.9	65.0	152.3

The methyl group of acetaldehyde can also facilitate β-C−H insertion from **B** (Figure 10 (path III) and Figure 13). The TS for this step **P** has the lowest of the three entrance barriers, lying 6.55 kcal/mol below the entrance to path II, and 12.9 kcal/mol below that for path I. An increasing Y−C_{CO} bond distance and a decreasing CC bond strength for $TS_{\beta CH}$ **P** is consistent with the formation of product **Q**, a hydride−enol species, the lowest point on the Y + CH_3CHO potential energy surface, ∼8 kcal/mol below the π complex **B**. The geometry of **Q** indicates a weak interaction between the CC π orbital and the metal. Like the first insertion intermediate in path II (**F**), **Q** can further react by several pathways. A hydride shift to the metal through TS_{CH}''' **R** or through $MCTS_{II}$ **S** occurs from the α-carbon and leads to the ketene species **L** and **M**, respectively, but the ordering of these two barriers is reversed relative to their counterparts in path II. Dissociative hydrogen atom loss is substantially endoergic and leads to the yttrium−enol species **T** with a linear Y−O−C bond. In contrast to product **O** from path II, which is overall endoergic from Y + MeHCO by 13.13 kcal/mol, the H atom elimination product **T** lies 8.80 kcal/mol *below* the reactant asymptote, making it accessible at all collision energies.

c. RRKM Branching Ratios for Pathways I, II, and III. The major products, $HYCH_3$ + CO, are produced from pathways I and II. In addition, these products may result from H_2Y(ketene) produced via channel III, followed by crossing to channel II. The minor products YCH_3CO + H and YCH_2CO + H_2 occur only through pathways II and III. The RRKM rate constants (Table 4) for each principal pathway were calculated from the CCSD(T)/BSII energies corrected for ZPE (BSII) and the B3LYP/BSII frequencies. The RRKM calculations were performed by using the π-complex **B** as the reactant, and **C**, **D**, and **P** each as tight transition states. Use of the π-complex **B** as the reactant is a reasonable assumption in light of the large π-complex **B** well depth and substantial barriers for subsequent reaction. At a collision energy of 7.1 kcal/mol, the branching ratio for pathways I:II:III was calculated to be k_{CC}:$k_{\alpha CH}$:$k_{\beta CH}$ = 1:4.30:13.92. As the collision energy is increased, the contribution from pathway I, and to a lesser extent, II, increased more rapidly than for III; the product ratio reached 1:3.25:5.19, at 26.8 kcal/mol.

i. CO Elimination. Due to interference from YO impurity present in the beam, which has the same *m*/*e* as $HYCH_3$, the absolute yield for this channel was only measured at one collision energy where deuterated acetaldehyde was used and the product detected was $DYCD_3$. The RRKM calculations provide insight into the relative importance of the three pathways

TABLE 5: Calculated CO Percent Yields and H:H_2 Elimination Branching Ratios for Y + CH_3CHO Reactions[a]

	%CO (CC)	%CO (αCH)	total %CO[b]	RRKM	exp
7.1	5.2	22.4	27.6	0.24:1.00	0.047:1.00
9.3	5.8	23.9	29.7	0.34:1.00	0.049:1.00
11.0	6.3	25.1	31.4	0.44:1.00	0.11:1.00
13.1	6.9	26.6	33.5	0.56:1.00	0.21:1.00
15.9	7.8	27.4	35.2	0.73:1.00	0.46:1.00
26.8	10.6	34.4	45.0	2.34:1.00	7.34: 1.00

[a] The RRKM H:H_2 branching ratios were calculated as k_{dissB}:$k_{MCTS-II}$. [b] Calculated as $(k_{cc} + k_{\alpha CH})/(k_{cc} + k_{\alpha CH} + k_{\beta CH})$.

in producing $HYCH_3$ + CO. Although pathway I leads solely to CO elimination, the relatively high C−C insertion barrier makes this route unfavorable, particularly at low collision energies, where only 5.2% of the reactions follow this pathway (Table 5). Although pathway III is dominant at all collision energies, it cannot be a significant source of CO, as this channel would require initial formation of H_2Y(ketene) (**L**) followed by C−H insertion via **I** producing **F** (i.e., by reversal of pathway II). Because the energy of **I** (pathway II) is substantially higher than that for **R** (pathway III), and because of the high barrier for direct H_2 elimination, H_2Y(ketene) should primarily isomerize to **Q**, followed by H or H_2 elimination. Although the barrier (**D**) for initial α-CH insertion on pathway II is higher than (**P**) for initial β-CH insertion on pathway III, pathway II primarily leads to $HYCH_3$ + CO due to the relatively low barrier height for subsequent C−C insertion (**G**). For path II, the low energy for $TS_{cc'}$ (**G**) leads to RRKM rate constants for $k_{CC'}$, which were orders of magnitude larger than k_{MCTS-I}. The rate constant k_{dissA} is nonzero only above E_{coll} = 15.9 kcal/mol. Thus, the fraction of π-complexes that produce $HYCH_3$ + CO at 7.1 kcal/mol is given by the ratio of rate constants $k_{\alpha CH} + k_{CC}/k_{\alpha CH} + k_{CC} + k_{\beta CH} = 0.224 + 0.052 = 0.276$. From the RRKM calculations, this yield is expected to increase to 0.449 at E_{coli} = 26.8 kcal/mol. As already noted, experimental CO yields are only available at E_{coli} = 24.6 kcal/mol for Y + CD_3CDO. The experimental value of 50.3% at this collision energy is in reasonably good agreement with the RRKM value (45.0%) calculated to be 26.8 kcal/mol.

ii. Branching Ratios for H and H_2 Elimination. As noted above, paths I and II only lead to CO elimination products, except at high collision energies where path II should also lead to the H atom channel (**O**), which is endoergic by 13.1 kcal/mol. Therefore, at E_{coll} < 13.1 kcal/mol, path III must be the sole source of H and H_2 elimination products, and the branching ratio for production of Y($OCHCH_2$) + H (**T**) to that for production of Y-ketene + H_2 (**M**) is simply the ratio of RRKM rate constants for H atom loss from **Q** yielding **T** to that for passage of intermediate **Q** to **M** over MCTS **S**, along pathway III. At E_{coll} = 7.1 kcal/mol, this ratio is 1.93:7.95 = 0.24:1.00, which is about a factor of 5 times larger than that observed experimentally. At a collision energy of 13.1 kcal/mol, this ratio is 9.42:16.8 = 0.56:1.00, which is a factor of 2.7 larger than the experimental value of 0.21:1.00. Thus, although the theoretical calculations reproduce the increase in relative H atom yield as the collision energy is increased, the RRKM calculations substantially overestimate the contribution from H atom fission at all collision energies except the highest. The discrepancy between the calculated and experimental H atom yield could be a result of either an underestimation of the endothermicity of H atom loss, or an overestimation of the theoretical barrier height **S**. It is also important to keep in mind the fact that the absolute branching ratio assumes that the photoionization cross sections are the same for both metal-containing products and are independent of the product internal energy. This assumption has been found to be reasonable in a previous study of the reaction of Y + propene,[35] based on comparisons with data taken using electron impact ionization detection, which may be calibrated. However, in the present work the signal levels are simply not large enough to allow for the use of electron impact detection. A calculation of the branching ratio at a collision energy of 26.8 kcal/mol yields a ratio of 71.6:65.0 = 2.34:1.00. At this collision energy, which is the highest studied experimentally, a very dramatic increase in H atom yield was observed, with the branching ratio increasing from 0.46:1.00 at E_{coll} = 15.9 kcal/mol to 7.34:1.00 at 26.8 kcal/mol. Thus, the theoretical calculations actually underestimate the H atom yield at the highest collision energy. In principle, this might be because the calculations have not explicitly included the endoergic H atom channel (**O**), which is energetically open at E_{coll} > 13.1 kcal/mol. According to the RRKM calculations, even at the highest collision energy, (**O**) is not expected to contribute significantly, despite the fact that α-C−H insertion increases relative to β-CH insertion with increasing energy. It remains possible, however, that the calculations underestimate the importance of this channel. Clearly, the H elimination channels (**O**) and (**T**) both proceed with no barrier in excess of the product endoergicity, whereas elimination of H_2 involves a barrier in the exit channel. Therefore, at low collision energies, H_2 elimination is dominant, but as the collision energy is increased, the rate constant for the H elimination channel should rise rapidly. The precise magnitude of this rise is very strongly dependent on the precise thermodynamics and on the details of the potential energy surfaces for the competing channels.

VI. Conclusions

The reactions of ground state Y (a^2D) with H_2CO and with CH_3CHO were studied at a range of collision energies in crossed molecular beams. For both molecular reactants, three product channels were observed, forming CO, H_2, and H. The experimentally measured branching ratios for competing pathways were compared to those predicted using RRKM theory, assuming competing reaction pathways following formation of π-association complexes involving the C=O bond. For acetaldehyde, reactions could proceed via three primary pathways, C−C insertion, α-C−H insertion, and β-C−H insertion. It was found that C−C insertion, a minor channel at all collision energies due to a relatively high-energy barrier, led exclusively to formation of $HYCH_3$ + CO. The α C−H insertion pathway also led to dominant formation of $HYCH_3$ + CO via a subsequent C−C insertion step. The α-C−H pathway also led to H atom production, but only at high collision energies. The dominant source of H and H_2 products at all collision energies involved π-complex formation followed by β-C−H insertion. Analysis of the β-C−H insertion pathway revealed a low-energy mechanism involving unimolecular rearrangement leading to production of Y-ketene + H_2 or production of the enol Y($OCHCH_2$) + H. In general, branching ratios calculated from RRKM rate constants were in reasonable agreement with the experimentally measured values.

Acknowledgment. This work was funded by the ACS Petroleum Research Fund and the National Science Foundation. J.S. thanks the Department of Education and the Cornell Graduate School for fellowships.

References and Notes

(1) Carroll, J. J.; Haug, L. K.; Weisshaar, J. C.; Blomberg, M. R. A.; Siegbahn, P. E. M.; Svensson, M. *J. Phys. Chem.* **1995**, *99*, 13955.

(2) Carroll, J. J.; Weisshaar, J. C.; Siegbahn, P. E. M.; Wittborn, C. A. M.; Blomberg, M. R. A. *J. Phys. Chem.* **1995**, *99*, 14388.

(3) Porembski, M.; Weisshaar, J. C. *J. Phys. Chem. A* **2000**, *104*, 1524.

(4) Porembski, M.; Weisshaar, J. C. *J. Phys. Chem. A* **2001**, *105*, 4851.

(5) Porembski, M.; Weisshaar, J. C. *J. Phys. Chem. A* **2001**, *105*, 6655.

(6) Stauffer, H. U.; Hinrichs, R. Z.; Willis, P. A.; Davis, H. F. *J. Chem. Phys.* **1999**, *111*, 4101.

(7) Stauffer, H. U.; Hinrichs, R. Z.; Schroden, J. J.; Davis, H. F. *J. Phys. Chem. A* **2000**, *104*, 1107.

(8) Willis, P. A.; Stauffer, H. U.; Hinrichs, R. Z.; Davis, H. F. *J. Phys. Chem. A* **1999**, *103*, 3706.

(9) Hinrichs, R. Z.; Schroden, J. J.; Davis, H. F. *J. Am. Chem. Soc.* **2003**, *125*, 861.

(10) Stauffer, H. U.; Hinrichs, R. Z.; Schroden, J. J.; Davis, H. F. *J. Chem. Phys.* **1999**, *111*, 10758.

(11) Bayse, C. A. *J. Phys. Chem. A* **2002**, *106*, 4226.

(12) Schroden, J. J.; Teo, M.; Davis, H. F. *J. Chem. Phys.* **2002**, *117*, 9258.

(13) Schroden, J. J.; Teo, M.; Davis, H. F. *J. Phys. Chem. A* **2002**, *106*, 11695.

(14) Li, T.; Cheng, W.; Liu, J.; Xie, X.; Cao, H. *J. Mol. Struct. (THEOCHEM)* **2006**, *761*, 83.

(15) Willis, P. A.; Stauffer, H. U.; Hinrichs, R. Z.; Davis, H. F. *Rev. Sci. Instrum.* **1999**, *70*, 2606.

(16) Powers, D. E.; Hansen, S. G.; Geusic, M. E.; Puiu, A. C.; Hopkins, J. B.; Dietz, T. G.; Duncan, M. A.; Langridge-Smith, P. R. R.; Smalley, R. E. *J. Phys. Chem.* **1982**, *86*, 2556.

(17) Proch, D.; Trickl, T. *Rev. Sci. Instrum.* **1989**, *60*, 713.

(18) Willis, P. A.; Stauffer, H. U.; Hinrichs, R. Z.; Davis, H. F. *J. Chem. Phys.* **1998**, *108*, 2665.

(19) Frisch, M. J.; Trucks, G. W.; Schlegel, H. B.; Scuseria, G. E.; Robb, M. A.; Cheeseman, J. R.; Montgomery, J. A., Jr.; Vreven, T.; Kudin, K. N.; Burant, J. C.; Millam, J. M.; Iyengar, S. S.; Tomasi, J.; Barone, V.; Mennucci, B.; Cossi, M.; Scalmani, G.; Rega, N.; Petersson, G. A.; Nakatsuji, H.; Hada, M.; Ehara, M.; Toyota, K.; Fukuda, R.; Hasegawa, J.; Ishida, M.; Nakajima, T.; Honda, Y.; Kitao, O.; Nakai, H.; Klene, M.; Li, X.; Knox, J. E.; Hratchian, H. P.; Cross, J. B.; Bakken, V.; Adamo, C.; Jaramillo, J.; Gomperts, R.; Stratmann, R. E.; Yazyev, O.; Austin, A. J.; Cammi, R.; Pomelli, C.; Ochterski, J. W.; Ayala, P. Y.; Morokuma, K.; Voth, G. A.; Salvador, P.; Dannenberg, J. J.; Zakrzewski, V. G.; Dapprich, S.; Daniels, A. D.; Strain, M. C.; Farkas, O.; Malick, D. K.; Rabuck, A. D.; Raghavachari, K.; Foresman, J. B.; Ortiz, J. V.; Cui, Q.; Baboul, A. G.; Clifford, S.; Cioslowski, J.; Stefanov, B. B.; Liu, G.; Liashenko, A.; Piskorz, P.; Komaromi, I.; Martin, R. L.; Fox, D. J.; Keith, T.; Al-Laham, M. A.; Peng, C. Y.; Nanayakkara, A.; Challacombe, M.; Gill, P. M. W.; Johnson, B.; Chen, W.; Wong, M. W.; Gonzalez, C.; Pople, J. A.; *Gaussian 03*, revision C.02; Gaussian, Inc.: Wallingford, CT, 2004.

(20) GAMESS-UK is a package of ab initio programs written by M. F. Guest, J. H. van Lenthe, J. Kendrick, K. Schoffel, and P. Sherwood, with contributions from R. D. Amos, R. J. Buenker, H. J. J. van Dam, M. Dupuis, N. C. Handy, I. H. Hillier, P. J. Knowles, V. Bonacic-Koutecky, W. von Niessen, R. J. Harrison, A. P. Rendell, V. R. Saunders, A. J. Stone, D. J. Tozer, and A. H. de Vries. The package is derived from the original GAMESS code due to M. Dupuis, D. Spangler and J. Wendoloski, NRCC Software Catalog, Vol. 1, Program No. QG01 (GAMESS), 1980.

(21) Woon, D. E.; Dunning, T. H. *J. Chem. Phys.* **1993**, *98*, 1358.

(22) Lajohn, L. A.; Christiansen, P. A.; Ross, R. B.; Atashroo, T.; Ermler, W. C. *J. Chem. Phys.* **1987**, *87*, 2812.

(23) Couty, M.; Hall, M. B. *J. Comput. Chem.* **1996**, *17*, 1359.

(24) Kendall, R. A.; Dunning, T. H.; Harrison, R. J. *J. Chem. Phys.* **1992**, *96*, 6796.

(25) (a) Stewart, R. F. *J. Chem. Phys.* **1970**, *52*, 431. (b) Langhoff, S. R.; Bauschlicher, C. W. *J. Chem. Phys.* **1986**, *84*, 4485.

(26) (a) Becke, A. D. *Phys. Rev.* **1988**, *A38*, 3098. (b) Lee, C.; Yang, W.; Parr, R. G. *Phys. Rev.* **1988**, *B37*, 785. (c) Colle, R.; Salvetti, O. *Theor. Chim. Acta* **1975**, *37*, 329.

(27) Kohn, W.; Sham, L. J. *Phys. Rev.* **1965**, *A140*, 1133.

(28) (a) Scuseria, G. E.; Scheiner, A. C.; Lee, T. J.; Rice, J. E.; Schaefer, H. F. *J. Chem. Phys.* **1987**, *86*, 2881. (b) Lee, T. J.; Rice, J. E. *Chem. Phys. Lett.* **1988**, *150*, 406. (c) Lee, T. J.; Rendell, A. P.; Taylor, P. R. *J. Chem. Phys.* **1990**, *94*, 5463.

(29) (a) Gilbert, R. G.; Smith, S. C. *Theory of Unimolecular and Rcombination Reactions*; Blackwell Scientific Publications: Oxford, U.K., 1990. (b) Baer, T.; Hase, W. L. *Unimolecular Reaction Dynamics*; Oxford University Press: New York, 1996. (c) Forst, W. *Theory of Unimolecular Reactions*; Academic Press: New York, 1973.

(30) Scoles, G. *Atomic and Molecular Beam Methods*; Oxford University Press: New York, 1998; Vol. 1, Chapter 1.

(31) Shimanouchi, T. *Molecular Vibrational Frequencies*; In NIST Chemistry WebBook; NIST Standard Reference Database Number 69; Linstrom, P. J., Mallard, W. G., Eds.; National Institute of Standards and Technology: Gaithersburg, MD, 20899; July 2001 (http://webbook.nist.gov).

(32) Zhu, L.; Hase, W. L. Program 644, Quantum Chemistry Program Exchange, Indiana University.

(33) For the Y + CH_3CHO RRKM calculations, the methyl group was treated as a torsional rotor, by dropping the lowest frequency vibrational mode and adding an internal rotor.

(34) (a) Miller, W. B.; Safron, S. A.; Herschbach, D. R. *Discuss. Faraday Soc.* **1967**, *44*, 108. (b) Miller, W. B.; Safron, S. A.; Herschbach, D. R. *J. Chem. Phys.* **1972**, *56*, 3581.

(35) Hinrichs, Z. R.; Schroden, J. J.; Davis, H. F. *J. Phys. Chem. A* **2003**, *107*, 9284.